Available online at www.sciencedirect.com

ScienceDirect

Procedia Structural Integrity 12 (2018) 281–295

Structural Integrity Procedia

www.elsevier.com/locate/procedia

AIAS 2018 International Conference on Stress Analysis

A novel composite bolted joint element: application to a single-bolted joint

Valerio G. Belardi[a], Pierluigi Fanelli[b], Francesco Vivio[a,*]

[a]*Department of Enterprise Engineering - University of Rome Tor Vergata, Via del Politecnico, 1, 00133, Rome, Italy*
[b]*Department of Economics, Engineering, Society and Business Organization, University of Tuscia, Largo dell'Università, 01100 Viterbo, Italy*

Abstract

Based on an analytical solution of the theoretical reference model of the composite bolted joint undergoing in-plane loads, a modeling technique for this kind of demountable connections is presented. The novel composite bolted joint element substitutes a region of the original model, comprising the bolt and the peripheral area, with a set of radially arranged beams: the cross-section properties are opportunely tailored in order to establish a stiffness equivalence between the theoretical reference model and the presented finite element through the resolution of a system of algebraic equations. The in-plane load condition is considered in this work because of its prevalence in comparison with other ones in many practical applications as the double lap shear joint. Numerical case studies are provided to validate the novel composite bolted joint element comparing FE models of circular plates, featuring a quasi-isotropic lay-up, with an internal rigid core or with the presented FE tool.

Keywords: rectilinear orthotropic composite material; circular plates; bolted connections

1. Introduction

Demountable joint connections represent a strategic connection method in the overall engineering fields. Moreover, the aeronautic and the aerospace fields are particularly sensible to the proper design of these structural elements and in the evaluation of their influence on the adjacent jointed components stress field, as testified by the published works related to the subject: in McCarthy et al. (2005); McCarthy and McCarthy (2005) a three-dimensional FE model is developed; the work by Gray and Mccarthy (2011) depicts the definition of a user-defined finite element to describe the load distribution of bolted composite structures; Kapidžić et al. (2014); Chowdhury et al. (2016) provided specific insights for aircraft structures applications.

Specifically, the necessities of developing efficient design tools for composite bolted joints is particularly relevant in aerospace design. As an example, considering anisogrid composite lattice structures that are progressively replacing

* Corresponding author. Tel.: +39 06 72597123.
E-mail address: vivio@uniroma2.it

2452-3216
10.1016/j.prostr.2018.11.087

metallic shells Belardi et al. (2018f,c), one of the main issues linked to their utilization is represented by the connection of their composite endings to metallic flanges through demountable joints.

Hereafter, an original FE modeling technique for composite bolted joints is presented. The methodology is founded on the new definition of a spot joint element, representative of the structural behavior of a region surrounding the spot joint. This joint element is based on the FE architecture of the Spot Joint Element, discussed in Vivio (2009) and able to simulate spot welded or riveted joint for metal sheets. The enhanced version implements a stiffness matrix whose terms are obtained according to the analytical solution of the composite bolted joint theoretical reference model.

The theoretical model consists in an annular plate, with rectilinear orthotropic material properties, featuring a rigid core at the inner radius and fully clamped conditions at the outer edge undergoing different external loads. Initial efforts towards the analytical solution of the problem are outlined by the authors in Belardi et al. (2018g,b). Overall, the theoretical background is obtained through an elaborate analytical procedure, based on Ritz method, necessary to solve the fundamental loading conditions acting on the bolted joint Belardi et al. (2018d,e,a): transversal load, in-plane load, in-plane bending moment and torsional moment.

The bolted joint element is realized through a suitable assembly of beam-type elements and it is representative of the structural behavior of a region surrounding the bolted joint, comprising the bolt and a circular portion of the connected plates. Furthermore, even if this FE tool features a reduced number of DOFs with respect to a complex 3D model, it preserves a substantial accuracy in the simulation of the bolted joint connection.

In the present work, the solution of the in-plane load condition of the theoretical reference model is outlined presenting the derivation of both the radial and the circumferential displacement components according to the energy based methodology which exploits Ritz method. Then, the bases of the structural equivalence of the theoretical reference model and the beam assembly that constitutes the Spot Joint Element, which allow to obtain an analogous stiffness between them, are provided as regards the stiffnesses related to the action of external loads acting on the plate mid-surface. In fact, in many technical applications, the more severe load acting on the bolted joint is represented by the shear load undergone by the connection. As an example, it could be taken into account one of the most extensively employed bolted joint configuration: the double lap shear joint, where the mutual interaction of the flanges makes negligible the bending load effects, especially on the central plate, with respect to the action of the in-plane shear load.

Moreover, the analogy concerning the in-plane stiffness terms is established by means of the proper definition of the beams cross-section properties.

The quasi-isotropic lay-up of the composite plates is considered in the work because of its wide employment in applications concerning composite bolted joints, as confirmed in McCarthy et al. (2005); McCarthy and McCarthy (2005); Gray and McCarthy (2010); Gray and Mccarthy (2011); Kapidžić et al. (2014); Zhou et al. (2015).

The results section depict a comparison between FE models of rectilinear orthotropic composite plates realized with traditional shell elements, featuring 4 nodes with 6 DOFs per node, that are employed as reference and models presenting the novel composite bolted joint. The effect of the aspect ratio of the novel composite bolted joint is investigated as long as the the bolt diameter one. The outcomes present a high degree of matching indicating an elevated accuracy of the proposed FE tool which can advantageously be utilized as an efficient design solution for the simulation of multi-jointed composite structures.

2. Constitutive equations

Rectilinear orthotropic composite circular plates are laminate made up of layers which possess fibers arranged along straight directions that make an angle with the x-axis of the global Cartesian coordinate system (see Fig. 1), as opposed to the case of circular orthotropic plates where the fibers are placed along the radial or the circumferential directions. As a consequence, this typology of plates are characterized by circumferentially variable material properties, because of the disposition of reinforcing fibers within the layers that make up the plate, along with axisymmetric geometry.

Therefore, because of the bending stiffnesses variability with the angular coordinate θ, the elastic linear analysis of rectilinear orthotropic composite plates turns out to be a bidimensional problem even for axisymmetric load conditions.

The stress-strain relation, defined in the cylindrical coordinate system (r, θ, z), in plane stress and strain conditions of the k^{th} rectilinear orthotropic layer composing the laminate circular plate is:

$$\begin{Bmatrix} \sigma_r \\ \sigma_\theta \\ \tau_{r\theta} \end{Bmatrix}_k = \left[\overline{Q}(\theta)\right]_k \begin{Bmatrix} \varepsilon_r \\ \varepsilon_\theta \\ \gamma_{r\theta} \end{Bmatrix}_k = \begin{bmatrix} \overline{Q}_{11}(\theta) & \overline{Q}_{12}(\theta) & \overline{Q}_{16}(\theta) \\ \overline{Q}_{12}(\theta) & \overline{Q}_{22}(\theta) & \overline{Q}_{26}(\theta) \\ \overline{Q}_{16}(\theta) & \overline{Q}_{26}(\theta) & \overline{Q}_{66}(\theta) \end{bmatrix}_k \begin{Bmatrix} \varepsilon_r \\ \varepsilon_\theta \\ \gamma_{r\theta} \end{Bmatrix}_k \tag{1}$$

where:

$$\left[\overline{Q}(\theta)\right]_k = \left[T(\theta)\right]\left[\overline{Q}\right]_k \left[T(\theta)\right]^T \tag{2}$$

is the transformed reduced stiffness matrix in the cylindrical coordinate system of the k^{th} rectilinear orthotropic layer, $\left[\overline{Q}\right]_k$ denotes the analogous stiffness matrix in the Cartesian coordinate system (x, y, z) and $\left[T(\theta)\right]$ is the coordinate system transformation matrix:

$$\left[T(\theta)\right] = \begin{bmatrix} \cos^2(\theta) & \sin^2(\theta) & 2\cos(\theta)\sin(\theta) \\ \sin^2(\theta) & \cos^2(\theta) & -2\cos(\theta)\sin(\theta) \\ -\cos(\theta)\sin(\theta) & \cos(\theta)\sin(\theta) & \cos^2(\theta) - \sin^2(\theta) \end{bmatrix} \tag{3}$$

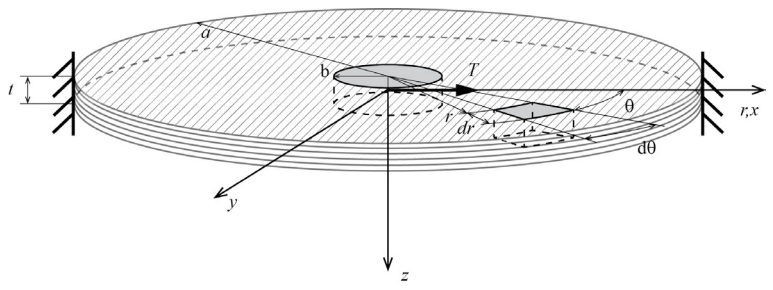

Fig. 1: Rectilinear orthotropic composite circular plate.

The terms of the matrix are no more constants, depending on the angular coordinate θ, as the layer exhibits a different elastic response according to the specific direction of the external load, they are:

$$\begin{aligned}
\overline{Q}_{11}^{(k)}(\theta) &= \overline{Q}_{11}^{(k)}c^4 + \left(\overline{Q}_{12}^{(k)} + 2\overline{Q}_{66}^{(k)}\right)2c^2s^2 + \left(\overline{Q}_{16}^{(k)}c^2 + \overline{Q}_{26}^{(k)}s^2\right)4cs + \overline{Q}_{22}^{(k)}s^4 \\
\overline{Q}_{12}^{(k)}(\theta) &= \overline{Q}_{12}^{(k)} + \left[\overline{Q}_{11}^{(k)} + \overline{Q}_{22}^{(k)} - 2\left(\overline{Q}_{12}^{(k)} + 2\overline{Q}_{66}^{(k)}\right)\right]c^2s^2 + \left[\left(\overline{Q}_{26}^{(k)} - \overline{Q}_{16}^{(k)}\right)c^2 + \left(\overline{Q}_{16}^{(k)} - \overline{Q}_{26}^{(k)}\right)s^2\right]2cs \\
\overline{Q}_{16}^{(k)}(\theta) &= \left[\left(\overline{Q}_{12}^{(k)} - \overline{Q}_{11}^{(k)} + 2\overline{Q}_{66}^{(k)}\right)c^2 + \left(\overline{Q}_{22}^{(k)} - \overline{Q}_{12}^{(k)} - 2\overline{Q}_{66}^{(k)}\right)s^2\right]cs + \overline{Q}_{16}^{(k)}c^2\left(1 - 4s^2\right) + \overline{Q}_{26}^{(k)}s^2\left(4c^2 - 1\right) \\
\overline{Q}_{22}^{(k)}(\theta) &= \overline{Q}_{22}^{(k)}c^4 + \left(\overline{Q}_{12}^{(k)} + 2\overline{Q}_{66}^{(k)}\right)2c^2s^2 - \left(\overline{Q}_{16}^{(k)}s^2 + \overline{Q}_{26}^{(k)}c^2\right)4cs + \overline{Q}_{11}^{(k)}s^4 \\
\overline{Q}_{26}^{(k)}(\theta) &= \left[\left(\overline{Q}_{22}^{(k)} - \overline{Q}_{12}^{(k)} - 2\overline{Q}_{66}^{(k)}\right)c^2 + \left(\overline{Q}_{12}^{(k)} - \overline{Q}_{11}^{(k)} + 2\overline{Q}_{66}^{(k)}\right)s^2\right]cs + \overline{Q}_{26}^{(k)}c^2\left(1 - 4s^2\right) + \overline{Q}_{16}^{(k)}s^2\left(4c^2 - 1\right) \\
\overline{Q}_{66}^{(k)}(\theta) &= \overline{Q}_{66}^{(k)} + \left(\overline{Q}_{11}^{(k)} + \overline{Q}_{22}^{(k)} - 2\left(\overline{Q}_{12}^{(k)} + 2\overline{Q}_{66}^{(k)}\right)\right)c^2s^2 + \left(\overline{Q}_{26}^{(k)} - \overline{Q}_{16}^{(k)}\right)\left(c^2 - s^2\right)2cs
\end{aligned} \tag{4}$$

being $c = \cos(\theta)$, $s = \sin(\theta)$.

The relations for the whole rectilinear orthotropic composite circular plate are derived from the stress-strain relation in Eq. (1). As stated by the classical plate theory (Jones (1975)), the displacement and strain fields are continuous along the plate thickness since the layers must be bonded together to be part of the same laminate, without the occurrence of relative slip between the layers which behave as a comprehensive elastic body. Consequently, the total laminate stresses are the sum of the homologous stress terms of all the N layers composing the rectilinear orthotropic composite circular plate:

$$\begin{Bmatrix} \sigma_r \\ \sigma_\theta \\ \tau_{r\theta} \end{Bmatrix} = \sum_{k=1}^{N} \begin{Bmatrix} \sigma_r \\ \sigma_\theta \\ \tau_{r\theta} \end{Bmatrix}_k = \sum_{k=1}^{N} \left[\overline{Q}(\theta)\right]_k \begin{Bmatrix} \varepsilon_r \\ \varepsilon_\theta \\ \gamma_{r\theta} \end{Bmatrix} = \left[\overline{Q}(\theta)\right] \begin{Bmatrix} \varepsilon_r \\ \varepsilon_\theta \\ \gamma_{r\theta} \end{Bmatrix} \tag{5}$$

in which the terms of the laminate reduced stiffness matrix are obtained as $\overline{Q}_{ij}(\theta) = \sum_{k=1}^{N} \overline{Q}_{ij}^{(k)}(\theta)$.

Moreover, the radial, circumferential and orthogonal displacement components of rectilinear orthotropic composite circular plate, evaluated along the coordinate directions r, θ and z are derived in accordance with the Kirchhoff-Love hypotheses for thin-plates:

$$\begin{cases} u_r(r,\theta,z) &= u(r,\theta) - z\dfrac{\partial w}{\partial r} \\ u_\theta(r,\theta,z) &= v(r,\theta) - z\dfrac{1}{r}\dfrac{\partial w}{\partial \theta} \\ u_z(r,\theta,z) &= w(r,\theta) \end{cases} \tag{6}$$

where u, v and w represent the radial, circumferential and orthogonal displacements of plate mid-surface ($z = 0$).

Furthermore, the strains related to the displacement field (6) are:

$$\begin{Bmatrix} \varepsilon_r \\ \varepsilon_\theta \\ \gamma_{r\theta} \end{Bmatrix} = \begin{Bmatrix} \dfrac{\partial u_r}{\partial r} \\ \dfrac{u_r}{r} + \dfrac{1}{r}\dfrac{\partial u_\theta}{\partial \theta} \\ \dfrac{1}{r}\dfrac{\partial u_r}{\partial \theta} + \dfrac{\partial u_\theta}{\partial r} - \dfrac{u_\theta}{r} \end{Bmatrix} = \begin{Bmatrix} \varepsilon_r^0 \\ \varepsilon_\theta^0 \\ \gamma_{r\theta}^0 \end{Bmatrix} + z \begin{Bmatrix} \kappa_r \\ \kappa_\theta \\ \kappa_{r\theta} \end{Bmatrix} = \begin{Bmatrix} \dfrac{\partial u}{\partial r} \\ \dfrac{u}{r} + \dfrac{1}{r}\dfrac{\partial v}{\partial \theta} \\ \dfrac{1}{r}\dfrac{\partial u}{\partial \theta} + \dfrac{\partial v}{\partial r} - \dfrac{v}{r} \end{Bmatrix} - z \begin{Bmatrix} \dfrac{\partial^2 w}{\partial^2 r} \\ \dfrac{1}{r}\left(\dfrac{\partial w}{\partial r} + \dfrac{1}{r}\dfrac{\partial^2 w}{\partial^2 \theta} \right) \\ 2\dfrac{\partial^2}{\partial r \partial \theta}\dfrac{w}{r} \end{Bmatrix} \tag{7}$$

in which every strain component features two contributions, the first one represents the mid-surface strains and the second one is related to the mid-surface curvatures. Stress resultants per unit width are obtained by means of the

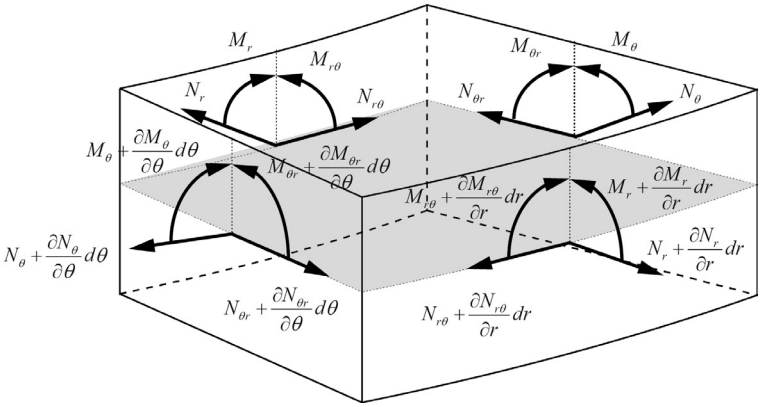

Fig. 2: Stress resultants acting on a plate element.

integration of elemental forces and moments in the laminate thickness t, over the N layers composing the composite circular plate. Thus, the resulting in-plane forces are (see Fig. 2):

$$\begin{Bmatrix} N_r \\ N_\theta \\ N_{r\theta} \end{Bmatrix} = \int_{-t/2}^{t/2} \begin{Bmatrix} \sigma_r \\ \sigma_\theta \\ \tau_{r\theta} \end{Bmatrix} dz = \sum_{k=1}^{N} \left[\overline{Q}(\theta) \right] \int_{z_{k-1}}^{z_k} \left(\begin{Bmatrix} \varepsilon_r^0 \\ \varepsilon_\theta^0 \\ \gamma_{r\theta}^0 \end{Bmatrix} + \begin{Bmatrix} \kappa_r \\ \kappa_\theta \\ \kappa_{r\theta} \end{Bmatrix} z \right) dz = \left[A(\theta) \right] \begin{Bmatrix} \varepsilon_r^0 \\ \varepsilon_\theta^0 \\ \gamma_{r\theta}^0 \end{Bmatrix} + \left[B(\theta) \right] \begin{Bmatrix} \kappa_r \\ \kappa_\theta \\ \kappa_{r\theta} \end{Bmatrix} \tag{8}$$

whereas the resulting radial and tangential bending moments and the torque moment turn out to be (see Fig. 2):

$$\begin{Bmatrix} M_r \\ M_\theta \\ M_{r\theta} \end{Bmatrix} = \int_{-t/2}^{t/2} \begin{Bmatrix} \sigma_r \\ \sigma_\theta \\ \tau_{r\theta} \end{Bmatrix} z dz = \sum_{k=1}^{N} \left[\overline{Q}(\theta) \right] \int_{z_{k-1}}^{z_k} \left(\begin{Bmatrix} \varepsilon_r^0 \\ \varepsilon_\theta^0 \\ \gamma_{r\theta}^0 \end{Bmatrix} z + \begin{Bmatrix} \kappa_r \\ \kappa_\theta \\ \kappa_{r\theta} \end{Bmatrix} z^2 \right) dz = \left[B(\theta) \right] \begin{Bmatrix} \varepsilon_r^0 \\ \varepsilon_\theta^0 \\ \gamma_{r\theta}^0 \end{Bmatrix} + \left[D(\theta) \right] \begin{Bmatrix} \kappa_r \\ \kappa_\theta \\ \kappa_{r\theta} \end{Bmatrix} \tag{9}$$

The circumferentially variable stiffness terms are:

$$A_{ij}(\theta) = \sum_{k=1}^{N} \overline{Q}_{ij}^{(k)}(\theta)(z_k - z_{k-1}) \qquad B_{ij}(\theta) = \frac{1}{2}\sum_{k=1}^{N} \overline{Q}_{ij}^{(k)}(\theta)(z_k^2 - z_{k-1}^2) \qquad D_{ij}(\theta) = \frac{1}{3}\sum_{k=1}^{N} \overline{Q}_{ij}^{(k)}(\theta)(z_k^3 - z_{k-1}^3) \quad (10)$$

where $A_{ij}(\theta)$ are the extensional stiffnesses, $B_{ij}(\theta)$ the bending-extension coupling stiffnesses and $D_{ij}(\theta)$ the bending stiffnesses for a rectilinear orthotropic composite circular plate expressed in the cylindrical coordinate system. In addition, z_k and z_{k-1} are the oriented distances to the bottom and the top, respectively, of the k^{th} layer.

3. Principle of virtual displacements and Ritz method

The presented solution methodology exploits the Ritz method Reddy (2006) that is applied in conjunction with the principle of virtual displacements:

$$\delta W = \delta W_I + \delta W_E = 0 = \int_\Omega \left(\sigma_r\, \delta\varepsilon_r + \sigma_\theta\, \delta\varepsilon_\theta + \tau_{r\theta}\, \delta\gamma_{r\theta}\right) d\Omega - \left(\int_\Omega \mathbf{f}\cdot\delta\mathbf{u}\, d\Omega + \int_{\Gamma_\sigma} \mathbf{T}\cdot\delta\mathbf{u}\, d\Gamma\right) \quad (11)$$

where δW_I and δW_E are, respectively, the internal and the external virtual works. The symbol δ is employed to identify virtual displacements and strains, Ω is the analytical integration region defining the rectilinear orthotropic composite circular plate, $\mathbf{f}$ denotes the body forces per unit volume, $\mathbf{T}$ the surface tractions per unit area acting on the external boundary portion Γ_σ.

Additionally, the expression of the internal virtual work of rectilinear orthotropic composite circular plates can be further specialized considering the strains dependence on the displacement components and performing an integration along the thickness direction:

$$\begin{aligned}\delta W_I = \int_b^a \int_{-\pi}^{\pi} \Bigg[& N_r \frac{\partial \delta u}{\partial r} + N_\theta\left(\frac{\delta u}{r} + \frac{1}{r}\frac{\partial \delta v}{\partial \theta}\right) + N_{r\theta}\left(\frac{1}{r}\frac{\partial \delta u}{\partial \theta} + \frac{\partial \delta v}{\partial r}\right) + \\ & - M_r \frac{\partial^2 \delta w}{\partial r^2} - M_\theta \frac{1}{r}\left(\frac{\partial \delta w}{\partial r} + \frac{1}{r}\frac{\partial^2 \delta w}{\partial^2 \theta}\right) - 2M_{r\theta}\frac{\partial^2}{\partial r \partial \theta}\frac{\delta w}{r}\Bigg] d\theta\, r dr\end{aligned} \quad (12)$$

Furthermore, Ritz method transfers the searching for the solution from the unknown displacement functions to a limited number of unknown coefficients c_j present in the discretized definition of the same displacement functions. Consequently, every unknown displacement component s must be written as a finite linear combination of approximation functions:

$$s \approx S_N = \varphi_0 + \sum_{j=1}^{N} c_j\, \varphi_j \quad (13)$$

In (13) the terms φ_j represents approximation functions. These approximation functions must be selected as a continuous, linearly independent and complete set of functions fulfilling the homogeneous form of the essential boundary conditions. On the contrary, φ_0 is the approximation function needed to satisfy the non-homogeneous essential boundary conditions if any is present, meanwhile the weights of the N approximation functions, i.e. the c_j coefficients, are the problem unknowns.

After the selection of the approximation functions and the substitution of the Eq. (13) in the Eq. (11), the principle of virtual displacements depends only on the N unknown coefficients and its validity must be assured for every admissible virtual displacement obtained with the δc_i coefficients:

$$\delta W(S_N) = \sum_{i=1}^{N} \frac{\partial W}{\partial c_i} \delta c_i = 0 \quad \forall \delta c_i \qquad \Rightarrow \qquad \frac{\partial W}{\partial c_i} = \sum_{j=1}^{N} R_{ij}\, c_j - F_i = 0, \quad i = 1, 2, \ldots, N \tag{14}$$

The validity of Eq. (14) requires the solution of a linear system of N algebraic equations to find the N unknown coefficients c_j. In addition, the coefficient matrix terms R_{ij} are dependent on the approximation functions, material properties and plate geometry, meanwhile the known terms F_i depend on the external loads.

3.1. Application to in-plane load condition

Hereafter, the algebraic equations system (14) is specialized to the in-plane load condition, i.e. an annular plate featuring a rigid core at the inner edge and a fully clamped constraint at the outer one made up of composite material with rectilinear orthotropic properties subject to an in-plane load T, applied in correspondence of the symmetry axis, acting on its mid-surface along the x-axis of the global Cartesian coordinate system (Fig. 2).

Accordingly, the external virtual work turns out to be:

$$\delta W_E = -\left(\frac{T}{2}\delta u(b, 0) - \frac{T}{2}\delta u(b, \pi)\right) \tag{15}$$

This expression was obtained keeping in mind that the application point of the in-plane load T does not belong to the annular plate integration domain Ω, so the external load was considered split in two contributions, acting along its direction, and applied at the inner radius b of the composite annular plate.

The stress resultants developed by this load condition on the composite annular plate are in-plane forces exclusively dependent on the mid-surface strains:

$$\begin{Bmatrix} N_r \\ N_\theta \\ N_{r\theta} \end{Bmatrix} = \begin{bmatrix} A_{11}(\theta) & A_{12}(\theta) & A_{16}(\theta) \\ A_{12}(\theta) & A_{22}(\theta) & A_{26}(\theta) \\ A_{16}(\theta) & A_{26}(\theta) & A_{66}(\theta) \end{bmatrix} \begin{Bmatrix} \varepsilon_r^0 \\ \varepsilon_\theta^0 \\ \gamma_{r\theta}^0 \end{Bmatrix} \tag{16}$$

In fact, as previously outlined, the composite annular plate is considered to have an uncoupled bending-extension behavior because of the theoretical background that is founded on the Classical plate theory which regards thin-plates and owing to the symmetric lay-up that makes to vanish the $\left[B(\theta)\right]$ stiffness matrix. As a result of these hypotheses, the action of the in-plane load T does not produce any moment stress resultant as well as no mid-surface transversal displacement w. Thus, the unknown displacement components to be determined are those along the radial and the circumferential direction, u and v respectively.

According to the theoretical reference model of composite bolted joints, the constraints imposed to the radial u and the circumferential v displacement components are:

$$(I)\ u(a, \theta) = 0 \qquad (II)\ v(a, \theta) = 0 \qquad (III)\ u(b, 0) = -v\left(b, \frac{\pi}{2}\right) \tag{17}$$

these boundary conditions considers the effects of the clamping conditions (*I*) and (*II*) and of the central rigid core at the inner edge of the plate (*III*).

The approximate forms of the in-plane displacement components u and v are:

$$\begin{aligned} u(r,\theta) &\approx U_N(r,\theta) = c_0\,\varphi_0(r,\theta) + \sum_{j=1}^{N} c_j\,\varphi_j(r,\theta) \\ v(r,\theta) &\approx V_M(r,\theta) = k_0\,\psi_0(r,\theta) + \sum_{l=1}^{M} k_l\,\psi_l(r,\theta) \end{aligned} \tag{18}$$

The employment of the φ_0 and ψ_0 approximation functions is related to the fact that at the inner radius the radial and the circumferential displacement components are other than zero but not known a priori.

The fulfillment of boundary conditions (17) require that: (*i*) the scalar coefficients $c_0 = k_0$ and (*ii*) a structure of the approximation functions which consists in the product of two functions − the first one exclusively depending on the radial coordinate r, equal for both the approximation functions $\varphi_{0,j}(r,\theta)$ and $\psi_{0,l}(r,\theta)$, and the second one that is a trigonometric function. Subsequently, the approximation functions are:

$$\begin{aligned} \varphi_{0,j}(r,\theta) &= p_{0,j}(r)\cos(\theta) \\ \psi_{0,l}(r,\theta) &= p_{0,l}(r)\Big(-\sin(\theta)\Big) \end{aligned} \tag{19}$$

The application of Ritz method to the principle of virtual displacements in (14) for the in-plane load condition returns the following system of algebraic equations that must be solved to determine the weight coefficients of the approximation functions:

$$\begin{bmatrix} R_{00}^{1x1} & R_{0j}^{1xN} & R_{0l}^{1xM} \\ R_{i0}^{Nx1} & R_{ij}^{NxN} & R_{il}^{NxM} \\ R_{k0}^{Mx1} & R_{kj}^{MxN} & R_{kl}^{MxM} \end{bmatrix} \begin{Bmatrix} c_0 \\ \vdots \\ c_j \\ \vdots \\ k_l \\ \vdots \end{Bmatrix} = \begin{Bmatrix} F_0 \\ \vdots \\ 0 \\ \vdots \\ 0 \\ \vdots \end{Bmatrix} \tag{20}$$

keeping in mind that the scalar coefficients c_0 and k_0 are equal. Furthermore, the terms in the coefficient matrix and the known terms vector of the system of algebraic equations (20) as well as the approximation functions for the displacement components are detailed in Belardi et al. (2018d).

4. Composite bolted joint finite element − in-plane stiffness matrix terms definition

The present work is focused on the definition of the stiffness matrix terms of the novel composite bolted joint element related to the in-plane load condition, i.e. on the identification of the stiffnesses along the radial r and the circumferential θ directions.

The novel composite bolted joint element is made up of a set of radial beams, featuring 6 DOFs per node, which replace a portion of preexisting shell elements mesh present in the overall FE model, as shown in Fig. 3. The set of radial beams lies on the composite plate mid-surface and it is equivalent from a structural point of view to the correspondent theoretical model. In addition, a single beam element exhibits the same stiffnesses of a circular sector

of the theoretical model having $\alpha_1 + \alpha_2$ angular extension with high degree of fidelity. The composite bolted joint element presents a very limited amount of DOFs, if compared to complex 3D models or even to shell models, and it is capable of improving the results accuracy with respect to approximate simulation techniques.

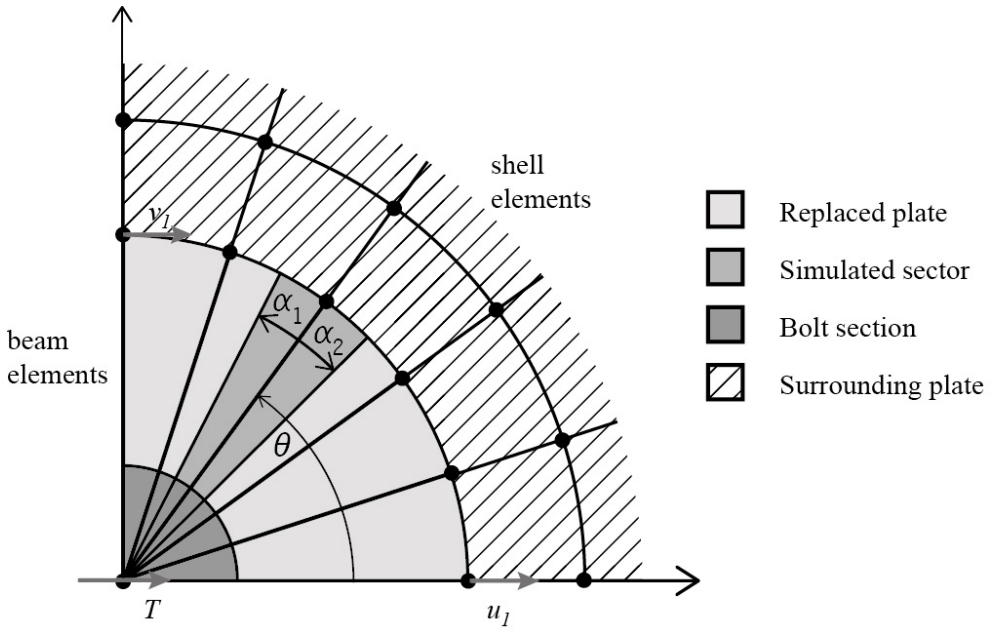

Fig. 3: Composite bolted joint element.

The stiffness equivalence between the theoretical reference model and the novel composite bolted joint element is obtained through the solution of a system of linear equations that is needed to determine the geometrical properties of the radial beams that must assure the structural equivalence which is established adjusting the beam cross-section properties in terms of inertia moment J_y and area A.

Consequently, the stiffnesses equivalence is obtained through the solution of the following system of algebraic equations that poses the equalities between the theoretical stiffness terms, defined as the ratio of a resulting generic force at the peripheral node and the displacement evaluated at the axis of the rigid nugget, and those related to the beam elements:

$$\begin{cases} K_{Fn_u}^{th} = K_{Fn_u}^{beam}\left(J_y\right) \\ K_{Ft_v}^{th} = K_{Ft_v}^{beam}\left(A\right) \end{cases} \tag{21}$$

Besides, $K_{Fn_u}^{th}$ and $K_{Ft_v}^{th}$ are evaluated as:

$$\begin{cases} K_{Fn_u}^{th} = \dfrac{Fn_2}{u_1} = \dfrac{a\int_{\alpha_1}^{\alpha_2} N_r(a,0)}{u(b,0)} \\ K_{Ft_v}^{th} = \dfrac{Ft_2}{v_1} = \dfrac{a\int_{\alpha_1}^{\alpha_2} N_{r\theta}\left(a,\frac{\pi}{2}\right)}{v\left(b,\frac{\pi}{2}\right)} \end{cases} \tag{22}$$

being the theoretical stiffness terms defined as:

- $K^{th}_{Fn_u}$ the ratio of the resultant radial in-plane loads Fn_2 on the outer border of the circular sector having extension $\alpha_1 + \alpha_2$ and centered on $\theta = 0$ − which is the maximum radial nodal loads − and the radial displacement at the nugget edge u_1.

- $K^{th}_{Ft_v}$ the ratio between the resulting tangential in-plane loads Ft_2 on the outer border of the circular sector having extension $\alpha_1 + \alpha_2$ and centered on $\theta = \frac{\pi}{2}$ − which is the maximum tangential nodal loads − and the tangential displacement at the rigid nugget edge v_1 for $\theta = \frac{\pi}{2}$ (v_1=u_1).

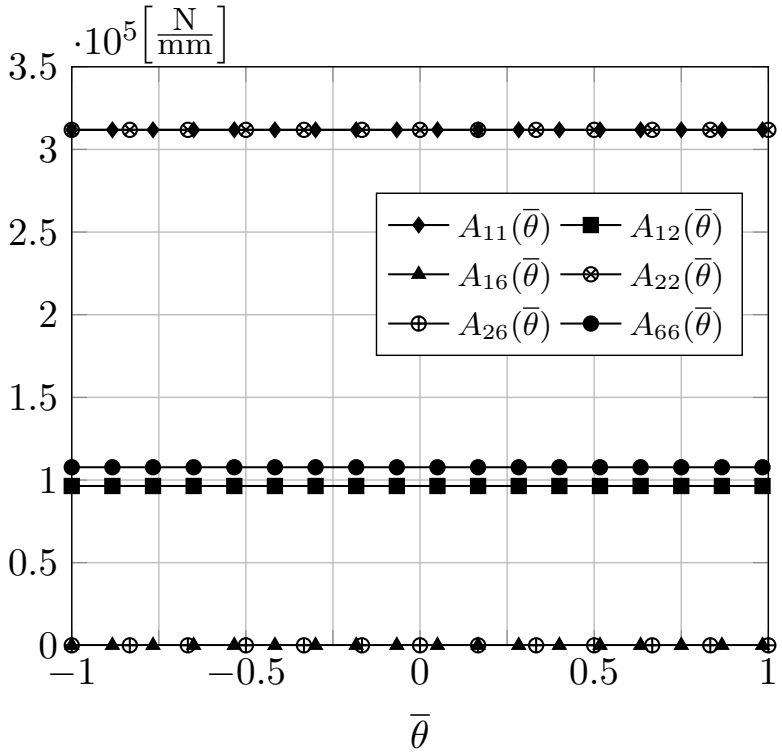

Fig. 4: Circumferential variation along the dimensionless angular coordinate $\overline{\theta}$ of the $A_{ij}(\theta)$ terms of the extensional stiffnesses matrix.

Moreover, as regards the lay-up considered in the Results section, i.e. the quasi-isotropic one (details can be found in Section 5), even though the plate is made up of composite material, the in-plane stiffness terms $A_{ij}(\theta)$ do not depend on the angular coordinate. Indeed, Fig. 4 outlines the dependence of the in-plane stiffness terms on the dimensionless angular coordinate $\overline{\theta}$, which shows a not appreciable circular variation. This aspect justifies the considerations regarding the employment of the maximum values of Fn_2 and Ft_2 in order to define the stiffness functions $K^{th}_{Fn_u}$ and $K^{th}_{Ft_v}$ which, as a consequence (see Eq. (22)), do not depend on the angular coordinate θ.

Likewise, the FE stiffness terms proper of the beam elements can be obtained considering the following relations deriving from the beam theory:

$$\begin{cases} K_{Fn_u}^{beam}\left(J_y\right) = \dfrac{EA}{a} \\ K_{Ft_v}^{beam}\left(A\right) = 12\dfrac{EJ_y}{a^3} \end{cases} \tag{23}$$

where E is the Young Modulus of the beam elements material.

5. Results

The results shown in this Section report the comparison between two variants of FE models of rectilinear orthotropic composite circular plates, featuring an internal rigid core: the first one realized with traditional FE modeling techniques and the second one with the novel composite bolted joint element. The load condition analyzed consists in an in-plane load T, of unitary intensity, acting on rigid nugget and along the x-axis of the global Cartesian coordinate system.

The plates thickness is $t = 5.2$ mm and they are characterized by quasi-isotropic lay-up: $[45/0/-45/90]_{5s}$; each layer has a thickness $t_{lay} = 0.13$ mm and mechanical properties listed are in Table 1.

Table 1: Unidirectional fiber-reinforced layer stiffness properties McCarthy et al. (2005).

E_{11} [GPa]	E_{22} [GPa]	E_{33} [GPa]	G_{12} [GPa]	G_{13} [GPa]	G_{23} [GPa]	ν_{12} [−]	ν_{13} [−]	ν_{23} [−]
140	10	10	5.2	5.2	3.9	0.3	0.3	0.5

The refined FE reference model is realized with layered shell elements featuring 4 nodes with 6 DOFs per node, whereas the internal rigid core is obtained by means of a material much more rigid than the composite one. Moreover, the FE reference model features an external radius $r_e = 24$ mm and two values of the bolt radius r_{bolt} were employed: 4 and 5 mm.

The FE models with the novel composite bolted joint are obtained through the replacement of a portion of the FE reference model that is substituted by the radial set of beams that composes the novel composite bolted joint, with cross-section properties obtained through Eq. (21).

In order to investigate the influence of the geometrical parameters on the results accuracy, different aspect ratios β between the internal and the external radii, b and a respectively, of the theoretical reference model (Fig. 1) were considered, i.e. $\beta_1 = 0.3, \beta_2 = 0.4$ and $\beta_3 = 0.5$.

Table 2: Radial displacement component evaluated at $\rho = 0$ with FE reference model u_{REF} and with FE model featuring the novel composite bolted joint element for various values β_i, between FE reference method and FE model with the novel composite bolted joint element.

r_{bolt} [mm]	$u_{REF} \cdot 10^5$ [mm]	$u_{\beta_1} \cdot 10^5$ [mm]	$u_{\beta_2} \cdot 10^5$ [mm]	$u_{\beta_3} \cdot 10^5$ [mm]
4	1.553	1.548	1.511	1.487
5	1.340	1.393	1.390	1.388

Table 2 outlines the radial displacements u evaluated alongside the external load T direction by means of the FE reference models and the ones featuring the novel composite bolted joint element, meanwhile the percentage errors between these values are depicted in Table 3.

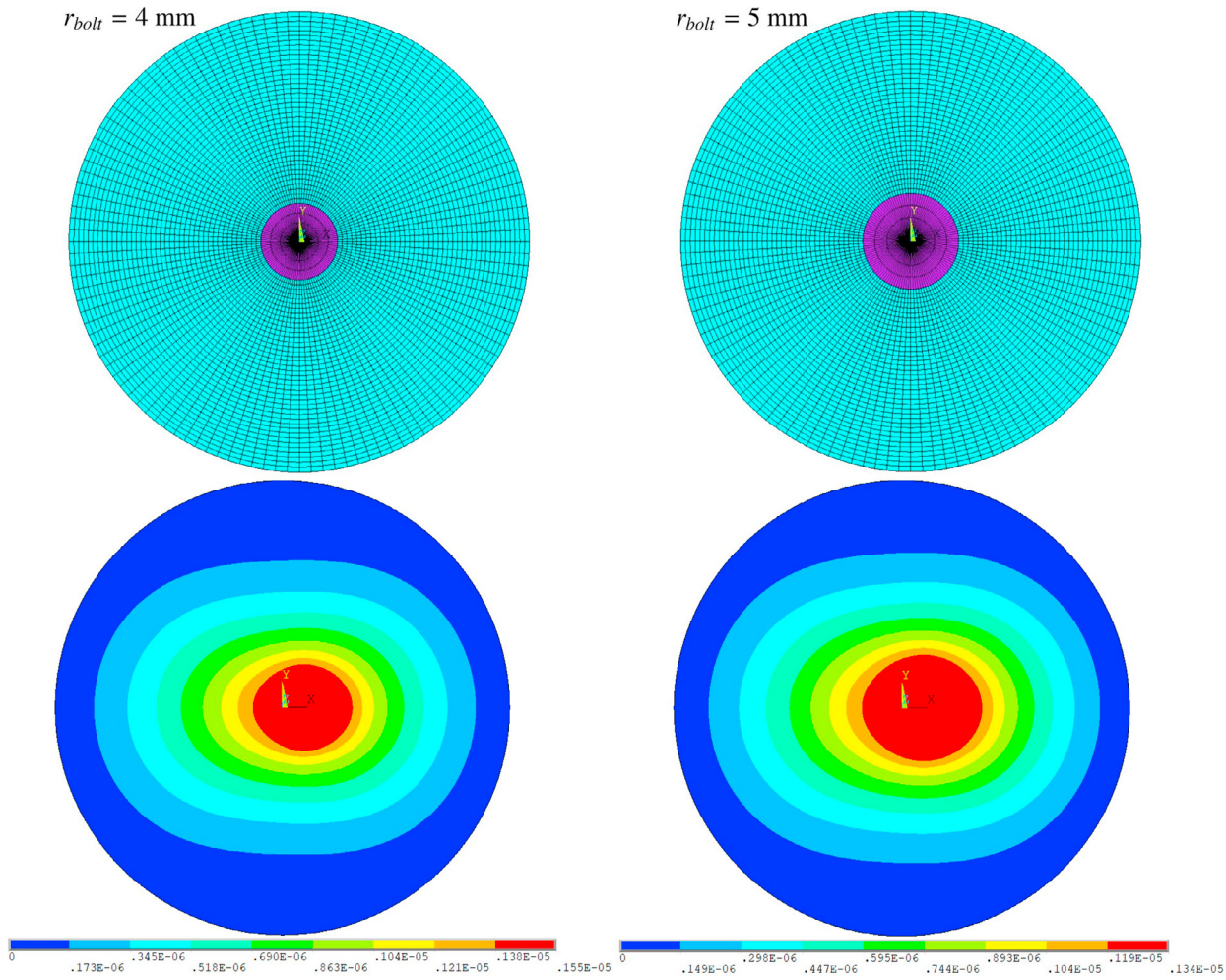

Fig. 5: FE reference models and contour of the displacement along the x-direction of the rectilinear orthotropic composite circular plates featuring r_{bolt} = 4 mm (left) and r_{bolt} = 5 mm (right).

Table 3: Radial displacement component percentage variation $\Delta_{\beta_i}[\%]$ evaluated at $\rho = 0$ for various values β_i, between FE reference method and FE model featuring the novel composite bolted joint element.

r_{bolt} [mm]	$\Delta_{\beta_1}[\%]$	$\Delta_{\beta_2}[\%]$	$\Delta_{\beta_3}[\%]$
4	−0.32	−2.70	−4.25
5	3.96	3.73	3.58

Besides, it can be concluded that, regardless of the specific geometrical configurations, the application of the novel composite bolted joint is capable of satisfactorily describing the structural behavior of the joint model as testified by the modest percentage errors.

Furthermore, it should be noted that such a remarkable level of results matching is realized through the adoption of meshes featuring a limited number of nodes and elements, with respect to the FE reference models, for all the aspect

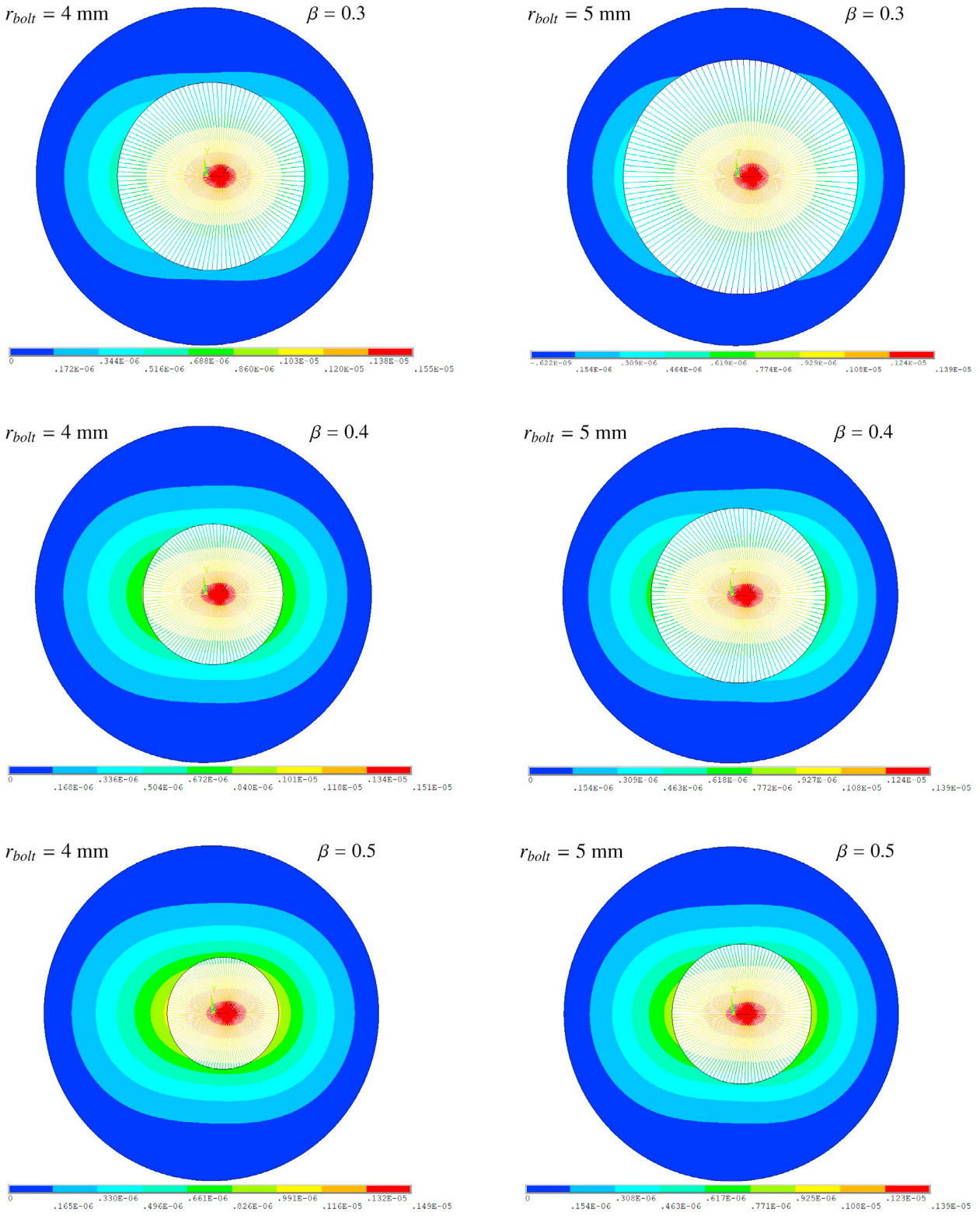

Fig. 6: FE models with the novel composite bolted joint element and contour of the displacement along the x-direction of the rectilinear orthotropic composite circular plates featuring r_{bolt} = 4 mm (left) and r_{bolt} = 5 mm (right).

Table 4: Node and element numbers of FE reference method and FE model featuring the novel composite bolted joint element with different aspect ratios β.

	REF	β_1	$\Delta_{\beta_1}[\%]$	β_2	$\Delta_{\beta_2}[\%]$	β_3	$\Delta_{\beta_3}[\%]$
Nodes	5041	1922	−61.9	2882	−42.8	3482	−30.9
Elements	5040	1920	−61.9	2880	−42.9	3480	−31.0

ratios considered, as listed in Table 4. Additionally, irrespective of the value of r_{bolt}, the two FE reference models and the FE models with the same aspect ratio β were realized by means of the same amount of nodes and finite elements.

Fig. 5 reports the FE reference models for the two values of r_{bolt} presenting the internal core made of rigid material properties and the contours relative to the displacement along the x-direction of the Global Cartesian coordinate system provoked by the external load T. Analogous contours are reported in Fig. 6 for the three FE models featuring the novel composite bolted joint element with different aspect ratios; the comparison of these result maps demonstrate that the overall stiffness of the models is equivalent to the reference one since the displacement distribution on the circular plates models can be superimposed to those in Fig. 5.

6. Conclusions

An accurate and computationally efficient FE tool for the modeling of composite bolted joints undergoing in-plane loads was presented. The sensibility of this simulation methodology against geometrical parameters was tested revealing a limited influence of these characteristics on the outcomes fidelity in the range of common applicability of the novel composite bolted joint element.

The presented model is capable of reproducing both the local displacement occurring on the bolt and the global displacement field of the plates in the area surrounding the bolted connection according to the proper definition of its stiffness matrix.

In the end, the proposed novel composite bolted joint element can be profitably exploited in the simulation of elaborate and computationally heavy FE simulations in order to reduce the model magnitude with no introduction of elevated and unacceptable approximations.

References

Belardi, V.G., Fanelli, P., Vivio, F., 2018a. Analysis of rectilinear orthotropic composite circular plates undergoing in-plane bending moment and torque through Ritz method. Composite Structures , under review.

Belardi, V.G., Fanelli, P., Vivio, F., 2018b. Bending analysis with Galerkin method of rectilinear orthotropic composite circular plates subject to transversal load. Composites Part B: Engineering 140, 250–259.

Belardi, V.G., Fanelli, P., Vivio, F., 2018c. Design, analysis and optimization of anisogrid composite lattice conical shells. Composites Part B: Engineering 150, 184–195.

Belardi, V.G., Fanelli, P., Vivio, F., 2018d. Elastic analysis of rectilinear orthotropic composite circular plates subject to transversal and in-plane load conditions using Ritz method. Composite Structures 199, 63–75.

Belardi, V.G., Fanelli, P., Vivio, F., 2018e. First-order shear deformation analysis of rectilinear orthotropic composite circular plates undergoing transversal loads. Under Review .

Belardi, V.G., Fanelli, P., Vivio, F., 2018f. Structural analysis and optimization of anisogrid composite lattice cylindrical shells. Composites Part B: Engineering 139, 203–215.

Belardi, V.G., Fanelli, P., Vivio, F., 2018g. Structural analysis of transversally loaded quasi-isotropic rectilinear orthotropic composite circular plates with Galerkin method. Procedia Structural Integrity 8, 368–378.

Chowdhury, N.M., Chiu, W.K., Wang, J., Chang, P., 2016. Experimental and finite element studies of bolted, bonded and hybrid step lap joints of thick carbon fibre/epoxy panels used in aircraft structures. Composites Part B: Engineering 100, 68–77.

Gray, P.J., McCarthy, C.T., 2010. A global bolted joint model for finite element analysis of load distributions in multi-bolt composite joints. Composites Part B: Engineering 41, 317–325.

Gray, P.J., Mccarthy, C.T., 2011. A highly efficient user-defined finite element for load distribution analysis of large-scale bolted composite structures. Composites Science and Technology 71, 1517–1527.

Jones, R.M., 1975. Mechanics of composite materials. Scripta Book Company Washington DC.

Kapidžić, Z., Nilsson, L., Ansell, H., 2014. Finite element modeling of mechanically fastened composite-aluminum joints in aircraft structures. Composite Structures 109, 198–210.

McCarthy, C.T., McCarthy, M.A., 2005. Three-dimensional finite element analysis of single-bolt, single-lap composite bolted joints: Part II effects of bolt-hole clearance. Composite Structures 71, 159–175.

McCarthy, M.A., McCarthy, C.T., Lawlor, V.P., Stanley, W.F., 2005. Three-dimensional finite element analysis of single-bolt, single-lap composite bolted joints: part I - model development and validation. Composite Structures 71, 140–158.

Reddy, J.N., 2006. Theory and analysis of elastic plates and shells. CRC press.

Vivio, F., 2009. A new theoretical approach for structural modelling of riveted and spot welded multi-spot structures. International Journal of Solids and Structures 46, 4006–4024.

Zhou, Y., Yazdani Nezhad, H., Hou, C., Wan, X., McCarthy, C.T., McCarthy, M.A., 2015. A three dimensional implicit finite element damage model and its application to single-lap multi-bolt composite joints with variable clearance. Composite Structures 131, 1060–1072.